Appl Phys A
DOI 10.1007/s00339-013-7604-8

Applied Physics A
Materials Science & Processing

Effect of ultrasonic treatment before and after hydrothermal process on the morphologies and formation mechanism of ZnO nanorods

J.J. Zhang · E.J. Guo · H.Y. Yue · L.P. Wang · C.Y. Zhang

Received: 4 October 2012 / Accepted: 31 January 2013

Abstract ZnO nanorods were fabricated by ultrasonic treatment before and after a hydrothermal process. The morphology and structure of the nanorods were individually characterized by scanning electron microscopy and X-ray diffraction. The results show that before the hydrothermal process, fore-ultrasonic treatment can directly gain ZnO nanorods which mainly experienced four conversion stages from initial bulk $Zn(OH)_2$, a coexisting phase of bulk $Zn(OH)_2$ with ZnO nanoslices, ZnO nanoslices with flower-like ZnO nanorods and finally to purely flower-like ZnO nanorods. After the hydrothermal process, the post-ultrasonic treatment mainly influences the aggregation degree of the ZnO nanorods. The formation mechanism of ultrasonic treatment on ZnO nanorods is also discussed.

1 Introduction

As a kind of important semiconducting oxide, nano-sized ZnO has potential applications in optoelectric devices, gas sensors, varistors, solar cells and other aspects by virtue of its unique physical and chemical characteristics [1–4]. The advantages of ZnO lie in its direct wide band gap of 3.3 eV, large exciton energy of 60 meV at room temperature, absorption of UV light, resistance to radiation, bio-safety properties and so on [5–7]. The stable crystal structure of ZnO is wurtzite structure composed of a number of alternating planes with tetrahedrally coordinated O^{2-} and Zn^{2+}, stacked alternately along the *c*-axis. The polar surfaces existing are prone to surface reconstruction to maintain stabilization and thus lead to the nanostructure's diversity.

Up to date, many techniques have been developed to fabricate one-dimensional nanomaterials, which mainly include thermal evaporation, chemical vapor deposition, sol–gel, hydrothermal treatment, solvo-thermal method, sonochemical synthesis and so on [8]. Among them, sonochemical synthesis has the advantages of homogeneous volumetric heating and high reaction rate [9]. The temperature and pressure inside the collapsing cavity could be high, up to 5000 K and 1800 atm, respectively, under the effect of intensive sonication [10]. Chen et al. [11] used the ultrasonic method to fabricate CeO_2 nanopowders with the diameter of 10 nm. The results indicated that ultrasonic radiation could expedite the reaction rate and refine CeO_2 nanoparticles effectively. Banerjee et al. [10] reported sonochemical preparation of ZnO nanoparticles from zinc acetate at the temperature of 65 °C without using any alkali for hydrolysis. It was found that the use of isopropanol was beneficial to synthesize the best crystalline ZnO. Wei and Chang [12] employed the ultrasonic method to synthesize ZnO nanoparticles in solutions containing different surfactants at room temperature. Anh et al. [13] reported that zinc hydroxide oxide could directly transform into zinc oxide by chemical reaction, but the conversion process from block-like zinc hydroxide oxide to ZnO nanorods was still not very clear and the detailed growth mechanism of ZnO nanorods was not investigated completely.

The hydrothermal process is an interesting method to fabricate diverse nanomaterials which has the advantages of simple procedures, easy control and low cost. However, as far as we know, no research of detailed ultrasonic treatment

Electronic supplementary material The online version of this article (doi:10.1007/s00339-013-7604-8) contains supplementary material, which is available to authorized users.

J.J. Zhang · E.J. Guo (✉) · H.Y. Yue · L.P. Wang · C.Y. Zhang
College of Materials Science and Engineering, Harbin University of Science and Technology, Harbin 150040, People's Republic of China
e-mail: guoerjun@126.com

Published online: 13 February 2013

combined with the hydrothermal process on the fabrication of ZnO nanorods was studied. Therefore, we try to investigate the effect of ultrasonic treatment before and after the hydrothermal process on the morphology and transformation mechanism of ZnO nanorods. In this paper, the effect of ultrasonic irradiation time on the morphology of ZnO nanostructures is mainly investigated and the possible formation mechanism of ZnO nanorods is also discussed. The gas sensing of ZnO nanorods is also investigated.

2 Experimental procedure

All the reagents were analytic grade and used without further purification. In a typical synthesis procedure, 4.5 mmol $Zn(NO_3)_2{\cdot}6H_2O$ and an equal molar ratio of $(CH_2)_6N_4$ (HMTA) were individually dissolved in 25 ml deionized water to form a transparent solution. After that, 25 ml NaOH aqueous solution with the molar quantity of 45 mmol was added dropwise to the above mixture under vigorous stirring. The resulting mixture was magnetically stirred for 5 min with the speed of 300 rpm and then was transferred into a 100 ml beaker and sealed with a plastic packing film. In order to investigate the effect of ultrasonic treatment on the growth of ZnO before the hydrothermal process, six samples were irradiated in an ultrasonic reactor (DS-7510DTH, ShangHai ShengXi Instrument Factory, 40 kHz, 450 W) under ambient air for different times of 0, 15, 30, 45, 60 and 90 min, respectively. Afterwards, the solution which had experienced 30 min ultrasonic irradiation was hydrothermally treated at 100 °C for 12 h and then was irradiated again for 0, 15 and 30 min, respectively. All as-prepared white precipitations were cleaned with 500 ml distilled water twice and then were centrifuged with the speed of 3000 rpm. Lastly, the white precipitations were dried at the temperature of 70 °C for 3 h to eliminate the adsorption water and collected for subsequent characterization and gas-sensing testing.

Before the hydrothermal process, the pH value of the solution was measured using a Mettler Toledo digital pH meter and the temperature of the solution after ultrasonic irradiation was detected by a common thermometer. The crystallographic structures were examined by X-ray diffraction (XRD, Philips X'Pert instrument) with monochromatized Cu-Ka radiation ($\lambda = 0.15406$ nm). The Bragg angle range used in the measurement was from 15° to 80° in scanning steps of 0.05°/s. The morphology and size distribution of the products were further observed by a scanning electron microscope (SEM, FEI-Sirion 200) operated at an acceleration voltage of 20 kV.

Gas sensing of ZnO nanorods that experienced post-ultrasonic treatment was also tested. The preparation process of the ZnO nanorod gas sensor is described as follows. Firstly, ZnO sensing materials were homogeneously mixed with appropriate quantities of terpineol and H_2PtCl_6. Subsequently, the mixture was coated onto the surface of ceramic tubes without covering the electrodes. A heater resistance was subsequently inserted into the ceramic tubes to render the working temperature of the sensors. Four Au electrodes of ceramic tubes and heater resistances were connected with the base of the sensor by welding. Afterwards, the made-up sensor was dried at 100 °C to remove the residual water and then put into an oven at the temperature of 350 °C for 2 h to remove the organics. To improve the stability and repeatability, the sensors were aged with the voltage of 3.5 V for 10 days in air prior to use. The relative response sensitivity was defined as R.S. $= (R_g - R_a)/R_a$, where R_a is the resistance in carrier gas and R_g is the resistance in a mixture gas of target gas (C_2H_5OH) and carrier gas. The time profile of gas response to adsorption and desorption of C_2H_5OH was recorded by a Labview data-collection system.

3 Results and discussion

3.1 Effect of ultrasonic irradiation before hydrothermal treatment on the morphology and formation mechanisms of ZnO nanorods

SEM morphologies of the samples synthesized by different times of ultrasonic treatment are shown in Fig. 1. It can be clearly seen that the morphology of the samples changes apparently with the increase of ultrasonic time. Figure 1a shows a kind of typical block-like morphology precipitate from the solution without the ultrasonic treatment. Figure 1b shows the mixed morphology of nanosize-slice and brick-like products simultaneously when the ultrasonic time reaches 30 min. Figure 1c shows that nanorods with the flower-like morphology have emerged among the slice product when the ultrasonic time increases to 45 min. With the prolongation of the ultrasonic time to 60 min, the proportion and dimension of flower-like nanorods increase gradually, as shown in Fig. 1d.

The XRD patterns of the fore-ultrasonic-treated samples are shown in Fig. 2. It depicts two kinds of different crystal products obtained during the different ultrasonic times. Figures 2a and b show the typical wulfingite $Zn(OH)_2$ characteristic peaks in agreement with the JCPDS card (No. 38-0385). Figure 2c represents a kind of mixed diffraction pattern which is identified as a $Zn(OH)_2$ and ZnO coexisting phase. Figure 2d shows the typical ZnO characteristic peaks with wurtzite structure according to the JCPDS card (No. 36-1451) without any peaks of impurities. The observed diffraction peaks of ZnO are assigned to (100), (002), (101), (102), (110), (103), (112) and (004), respectively. The average crystallite size of the ZnO nanorods is calculated to

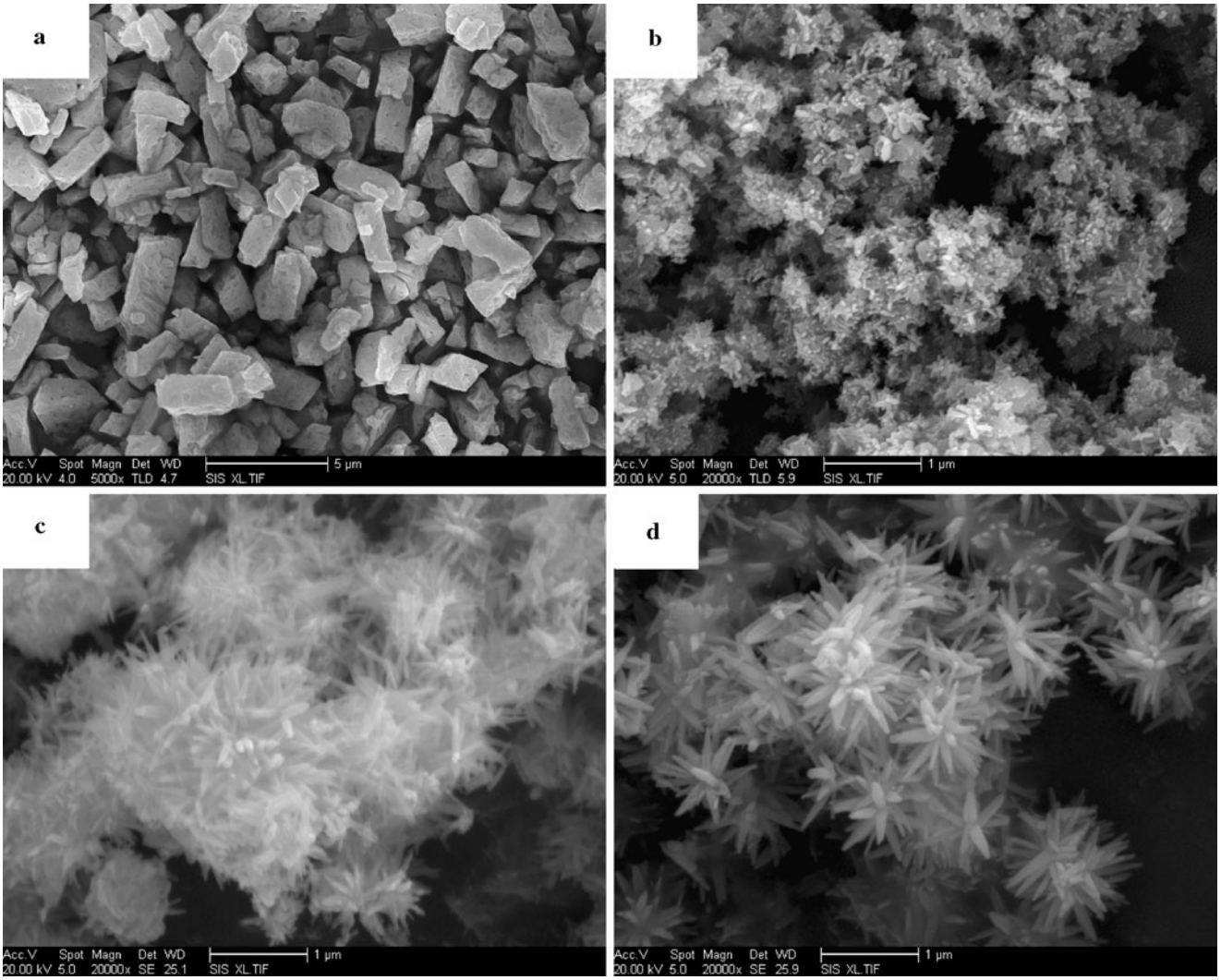

Fig. 1 SEM images of ZnO samples under ultrasonic treatment with different times. (**a**) 0 min, (**b**) 30 min, (**c**) 45 min, (**d**) 60 min

be about 55 nm using the Scherrer formula ($d = k\lambda/\beta\cos\theta$, where d is the mean crystallite size of the product, λ is the wavelength of the Cu-Ka radiation, β is the full width at half-maximum (FWHM) intensity of the (101) peak in radians, θ is Bragg's diffraction angle and k is a constant usually equal to 0.9).

The curves of solution pH and temperature are shown in Fig. 3. It can be seen that the pH value of the solution continuously declines and the temperature of the solution goes up with increasing ultrasonic time. It is well known that the ultrasonic irradiation is beneficial to promote the chemical reaction occurring in the solution, accelerating the mass transfer of the reactive substance, especially for the reason that the high temperature produced during cavitation can rupture chemical bonds and facilitate the crystallization of the product [14]. Consequently, it demonstrates that the raw materials of NaOH and HMTA participate in the reaction and are consumed constantly with elongation of the ultrasonic time, as shown in Eqs. (1)–(3).

The formation procedure and growth mechanism of ZnO can be explained by the sonochemical effect that has been refined to fabricate several kinds of nanomaterials with much smaller sizes and higher surface areas. It is known that the sonochemical effect originates from the acoustic cavitation which includes three discrete stages: nucleation, bubble growth and implosive collapse [15]. Suslick et al. [16] have pointed out that there are two regions of sonochemical activity involving the inside of the collapsing bubble, and the interface between the bubble and the liquid. The rapid compression of gas during cavitation collapse leads to the formation of a localized hot spot in the liquid. This cavitation hot spot causes bond cleavage or rearrangement, followed by atomic and radical recombination, and thermal and chemical quenching [17].

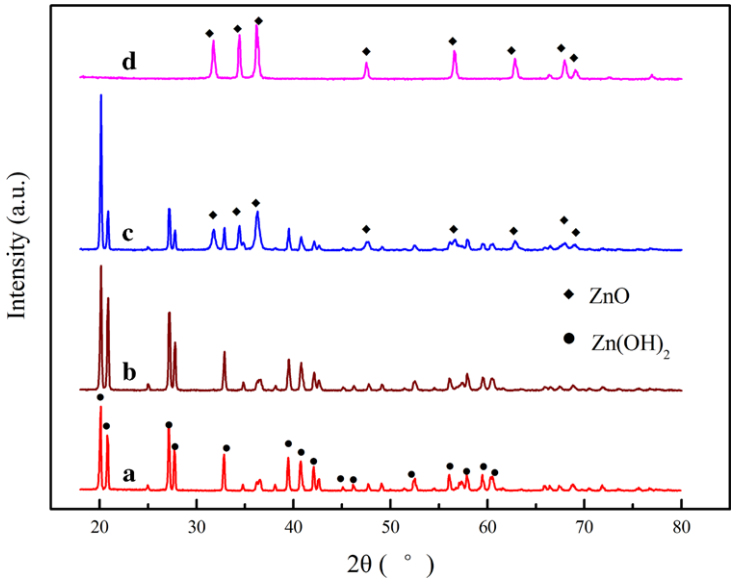

Fig. 2 XRD patterns of the samples under ultrasonic treatment for different times. (**a**) 0 min, (**b**) 30 min, (**c**) 45 min, (**d**) 60 min

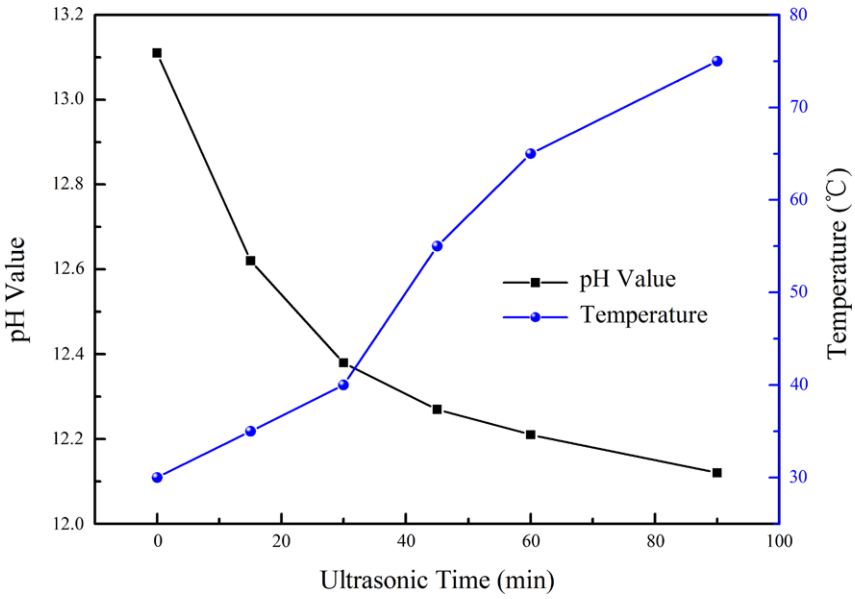

Fig. 3 Curves of pH and temperature of the solution with different ultrasonic times

At the starting stage of the reaction, $Zn(OH)_2$ colloid formed the cavitation bubbles, which are activated in the solution, break and release energies to form an active site on the surface of the Zn atom. The primary products of the sonication solution may be $Zn^{\bullet}$, $^{\bullet}OH$, $^{\bullet}O_2$, $^{\bullet}HO_2$ and $^{\bullet}H$, radicals formed within the collapsing gas bubble [18]. As strong oxidant radicals, $^{\bullet}OH$ and $^{\bullet}O_2$ can promote the growth of ZnO nanomaterials through the intermediate product of zinc hydroxide [19].

In our experiment, we think that zinc hydroxide maybe directly fulfills this decomposition by the ultrasonic effect. It is relevant to the effect of the sound radical ion produced in the solution. The interaction energy between the surface of zinc oxide and the radical ion would destroy the chemical bond of zinc hydroxide, a part of the Zn atom would break away from the original body and enter into the solution by the ion form. The Zn ion would react with the OH^- existing in the solution and form $Zn(OH)_4^{2-}$ according to Eqs. (3) and (4). The $Zn(OH)_4^{2-}$ will continue to change into the nuclei of zinc oxide according to Eq. (5). Some of the $Zn(OH)_2$ reacts with the excessive OH^- to form $Zn(OH)_4^{2-}$ [20]. The other Zn atoms would keep ion morphology and have chance to meet the radical ion in the solution, and the reaction is illustrated in Eqs. (5) and (6). The other $Zn(OH)_2$ can be directly decomposed into $Zn^{\bullet}$ and OH^- by the interaction of the radical ion and finish the process of changing into ZnO according to Eqs. (6) and (7).

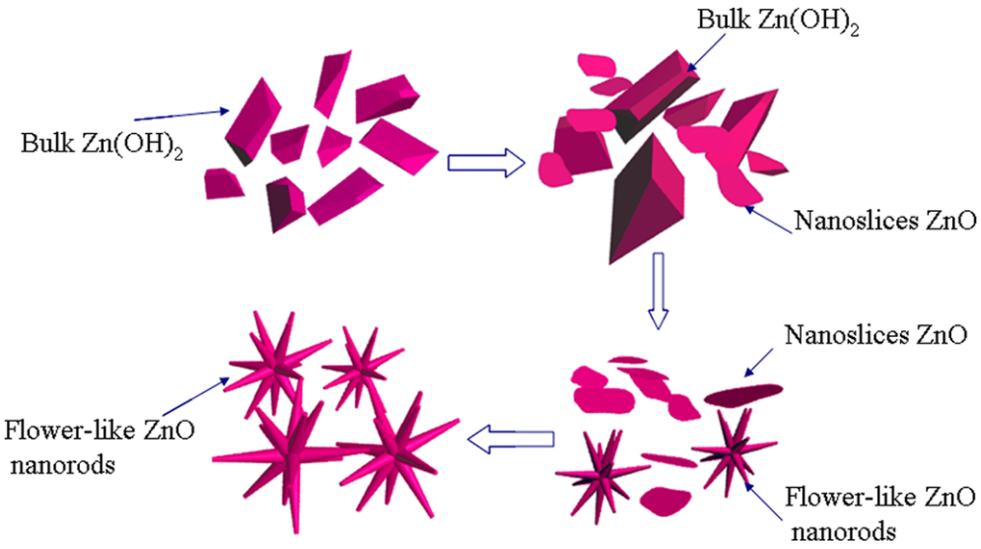

Fig. 4 Morphology evolution illustration of ZnO nanorods under ultrasonic irradiation

In general, the possible sonochemical growth mechanism of ZnO nanostructures is as follows [12, 16]:

$$(CH_2)_6N_4 + 6H_2O \rightarrow 4NH_3 + 6HCHO \quad (1)$$

$$NH_3 + H_2O \rightarrow NH_4^+ + OH^- \quad (2)$$

$$Zn^{2+} + 2OH^- \rightarrow Zn(OH)_2 \downarrow \quad (3)$$

$$Zn(OH)_2 \downarrow + 2OH^- \rightarrow \left[Zn(OH)_4\right]^{2-} \quad (4)$$

$$\left[Zn(OH)_4\right]^{2-} \rightarrow ZnO + 2H_2O + \frac{1}{2}O_2 \quad (5)$$

$$Zn^{\bullet} + 2^{\bullet}O_2^- \rightarrow ZnO + \frac{3}{2}O_2 \quad (6)$$

$$Zn^{\bullet} + {}^{\bullet}OH^- \rightarrow ZnO + {}^{\bullet}H \quad (7)$$

The above results make the nuclei directionally aggregate and assemble under the inducement of HMTA within the collapsing bubbles; ZnO nuclei form and grow into nanoparticles within the collapsing bubbles. Finally, zinc hydroxide would partly change into slice nanoparticles of ZnO. With the elongation of the ultrasonic time, the slice particles will further decompose and transform into ZnO nanorods. The decomposition may start from the exterior of $Zn(OH)_2$ and gradually moves to the interior of the particle. If the energy provided by the ultrasonics is high enough to fulfill this kind of decomposition, then the above decomposition will proceed continuously. On increasing the ultrasonic time, the new nuclei will recombine and exhibit polarity growth behavior. These formed fresh nuclei in the solution are unstable and have a tendency to grow into larger particles. Simultaneously, there is a large number of dangling bonds, defects or traps on the nuclei surface. With the aid of ultrasonic energy, these unstable nuclei can grow themselves in certain facets leading to the flower-like rods.

The complete conversion process of ZnO nanorods fabricated by fore-ultrasonic treatment is illustrated in Fig. 4. This collapse occurs in less than a nanosecond, at very high cooling rates [21, 22]. So, we can conclude that the polar growth of ZnO nanorods would be inhibited by high cooling rates rendered by ultrasonic irradiation so as to hinder the further organization and crystallization of the products. Thus, the length of the ZnO nanorods will be limited to a certain extent and not continuously increase.

3.2 Effect of post-ultrasonic treatment on the morphology of ZnO nanorods

As an n-type semiconductor oxide, ZnO shows very high sensitivity to many reducing gases, such as H_2, CO and C_2H_5OH. But, the sensitivity of a gas sensor is not only relevant to the physics properties but also to the surface morphology and distribution of materials. It is believed that sensor sensitivity can be improved by increasing the sensor surface area in order to provide more surface sites available for more oxygen to be adsorbed on these sites and to make contact with the surrounding gases [23]. In our opinion, the aggregated morphology of flower-like ZnO nanorods may limit the expanding of the contact surface. Hence, we try to scatter flower-like nanorods by the post-ultrasonic technique in order to improve the gas sensing of the ZnO sensor.

Figure 5 depicts the different morphologies of ZnO nanorods after the hydrothermal process. Figure 5a shows the morphology of ZnO nanorods fabricated by hydrothermal treatment at 100 °C for 12 h with fore-ultrasonic treatment for 30 min and without the post-ultrasonic treatment. As can be seen, the lengths of the ZnO nanorods increase from 500 nm to 3–5 μm and the diameters also increase from 50 nm to 150–200 nm. Compared with the ultrasonic treatment, the product exhibits good flower-like morphology.

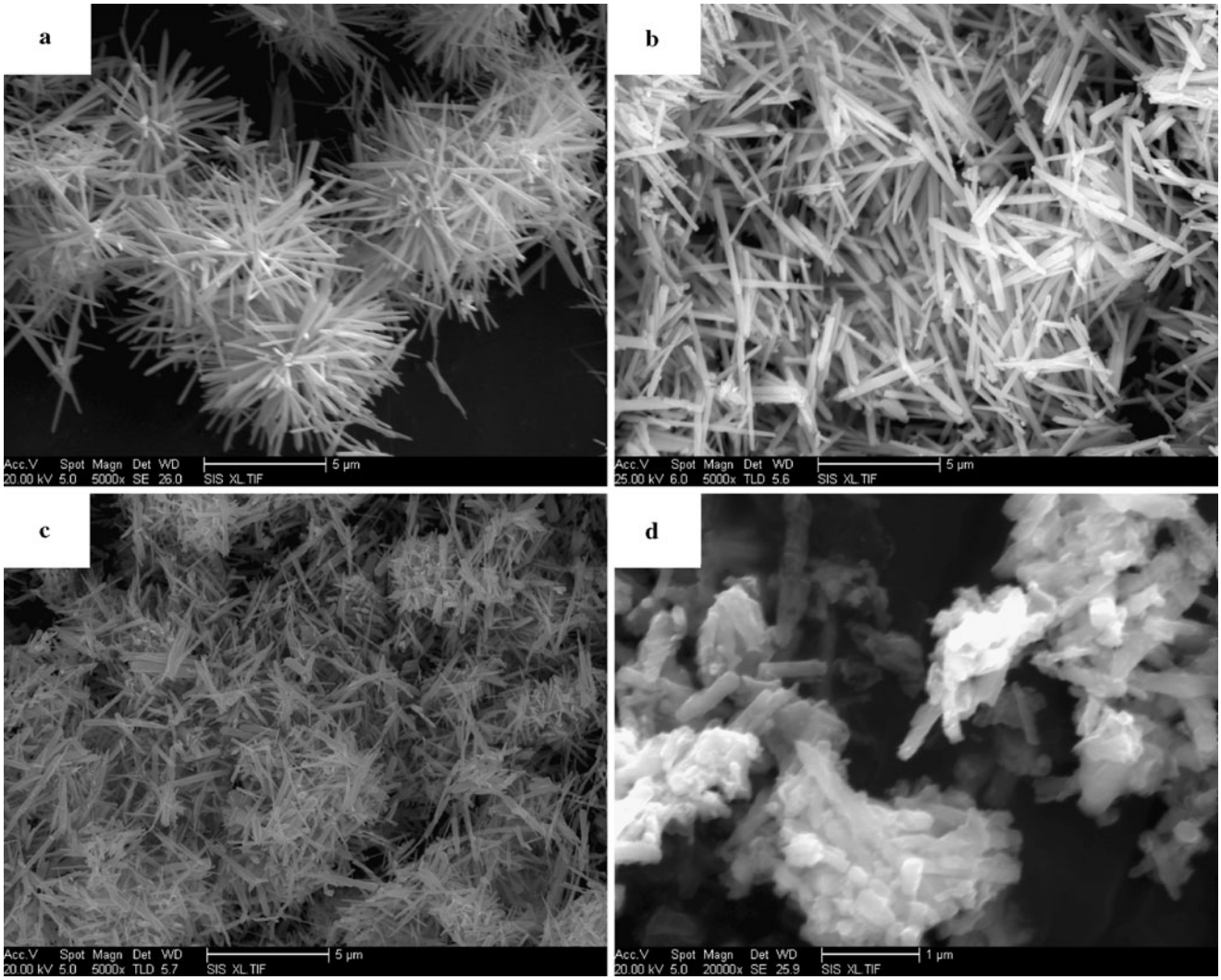

Fig. 5 SEM images of ZnO nanorods obtained by hydrothermal method after post-ultrasonic treatment for different times. (**a**) 0 min, (**b**) 15 min, (**c**) 30 min, (**d**) without fore-ultrasonic and post-ultrasonic treatment

This could be elucidated by the growth mechanism of hydrothermal treatment, which can promote further growth of ZnO nanorods [24]. With the increase of post-ultrasonic irradiation time, the original flower-like morphology of the ZnO nanorods is destroyed. When the ultrasonic time reaches 45 min, it shows an over-aggregated morphology, as shown in Fig. 5c. It indicated that the combination force of flower-like ZnO nanorods is not too much and nanorods can be further agglomerated by the energy of the ultrasonic treatment. For comparison, the experiment of solely hydrothermal treatment at 100 °C for 12 h without the aid of fore-ultrasonic treatment was carried out. The SEM image of ZnO as-prepared nanorods is shown in Fig. 5d. It can be seen that the prepared products are ZnO nanorods with a diameter of 50–70 nm and a relatively shorter length. The ZnO nanorods are adjacent to each other and aggregate to a certain extent. Compared with the samples which underwent fore-ultrasonic treatment, we find that the process of fore-ultrasonic treatment combined with hydrothermal treatment is more beneficial to gain a uniform and well-dispersed flower-like morphology of ZnO nanorods. It is relevant to the formation of ZnO primary nuclei during the fore-ultrasonic process. This also provides us with an effective method to gain nanorods with different dispersed degrees by post-ultrasonic treatment.

3.3 Gas sensing of ZnO nanorods to C_2H_5OH gas

We also investigated the gas sensing of ZnO nanorods after post-ultrasonic treatment for 15 min. The sensor is firstly exposed to 20 ppm C_2H_5OH at different operating temperatures in order to find the optimum operating temperature, as shown in Fig. 6. The response of the sensor firstly increases and then decreases with increasing operating temperature.

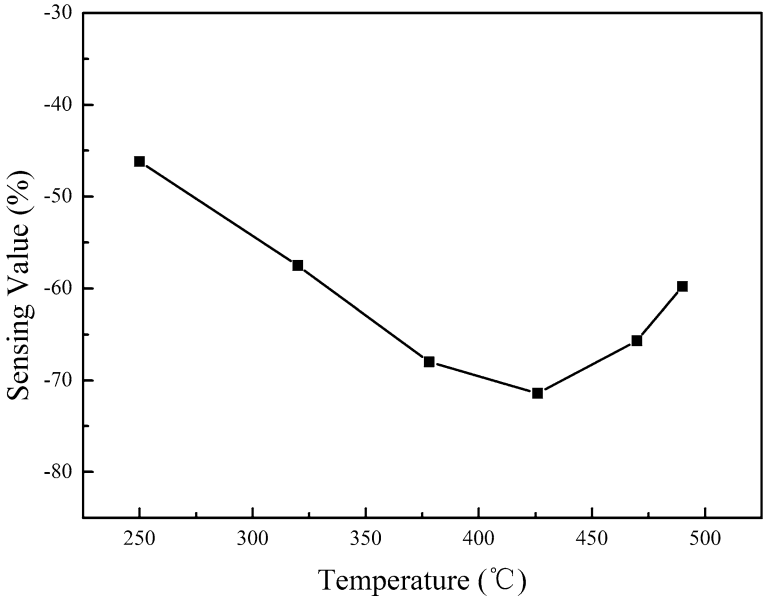

Fig. 6 Gas-sensing curves of ZnO nanorods to C_2H_5OH gas at different working temperatures

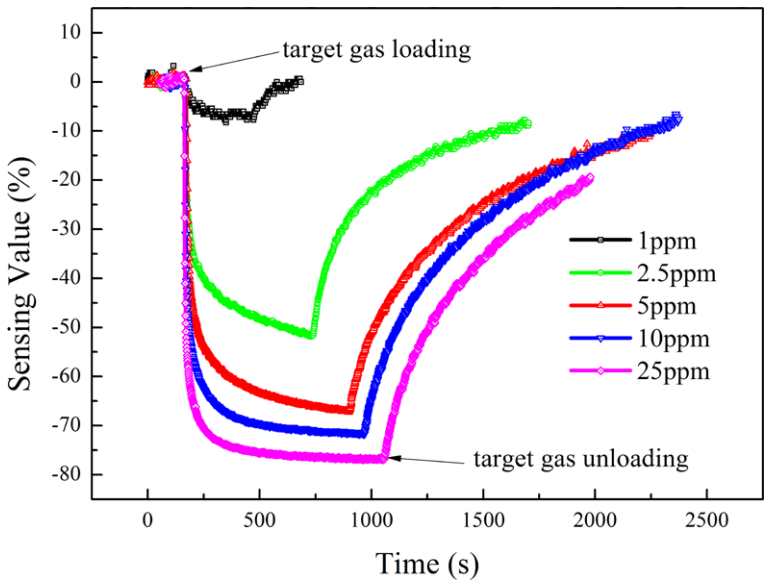

Fig. 7 Gas-sensing curves of ZnO nanorods to C_2H_5OH gas with different concentrations

The maximum value of the gas response is 71.4 % at the operating temperature of 425 °C.

Figure 7 shows the response of the scattered ZnO nanorod sensor exposed to different concentrations of C_2H_5OH gas at the temperature of 425 °C. The gas-sensing value increases gradually with increasing concentration of C_2H_5OH gas. The increasing amplitude of the sensing value is higher at low detective concentration than at higher concentration. The maximum response value of the ZnO nanorod sensor can reach 76.3 % for 25 ppm C_2H_5OH gas. When the concentration of C_2H_5OH gas is 2.5 ppm, the sensor has a distinct resolution capability. In addition, the dynamic response of the scattered ZnO nanorods to different concentrations of ethanol displays good response and recovery properties for ZnO nanorod-based sensors. All the response times and recovery times of the sensors at the ethanol concentrations of 5, 10 and 15 ppm are less than 40 s. Xu et al. [25] had also studied the gas sensing of ZnO nanorods synthesized by the hydrothermal process. Compared to their results, we found that the sensor made by scattered ZnO nanorods had lower detection limitation and better gas sensitivity to the same concentration of C_2H_5OH gas.

The sensing mechanism of ZnO nanorods to C_2H_5OH gas can be explained similar to the theory of the space-charge model, in that the change of resistivity is related to the chemical reaction kinetics between C_2H_5OH gas molecules and oxygen ions adsorbed on the surface of the nanorods [2]. Thus, the scattered ZnO nanorods can be used as a promising material for C_2H_5OH-sensing sensors.

4 Conclusions

The effect of ultrasonic treatment on the synthesis of ZnO nanorods combined with the hydrothermal method was investigated. Before the hydrothermal process, fore-ultrasonic treatment can directly gain ZnO nanorods which mainly experienced four conversion stages from initial bulk $Zn(OH)_2$, a coexisting phase of bulk $Zn(OH)_2$ with ZnO nanoslices, ZnO nanoslices with flower-like ZnO nanorods and finally to purely flower-like ZnO nanorods. An appropriate fore-ultrasonic treatment time is beneficial to form the nucleus of ZnO nanorods with the length of 50–75 nm and the diameter of 30–45 nm. The effect of post-ultrasonic treatment on the morphology of the ZnO nanorods was also studied. The result indicates that post-ultrasonic treatment can destroy the flower-like morphology of the ZnO nanorods from dispersion to an over-aggregation state with the elongation of the ultrasonic time. Scattered ZnO nanorods fabricated by the hydrothermal process with post-ultrasonic treatment exhibit a promise sensing to C_2H_5OH gas.

Acknowledgements This work is supported by the National Natural Science Foundation of China (No. 51201052), the Special Fund for Scientific and Technological Innovative Talents in Harbin City (No. 2012RFQXG107) and the Natural Science Foundation of Heilongjiang Province of China (No. E201056).

References

1. X. Wang, X. Wang, C.J. Summers, Z.L. Wang, Large-scale hexagonal-patterned growth of aligned ZnO nanorods for nano-optoelectronics and nanosensor arrays. Nano Lett. **4**, 423–426 (2004)
2. S.R. Mahmoodi, B. Raissi, E. Marzbanrad, N. Shojayi, A. Aghaei, C. Zamani, Dielectrophoretic assembly of ZnO nanorods for gas sensing. Procedia Chem. **1**, 947–950 (2009)
3. R. Subasri, M. Asha, K. Hembram, G. Rao, T.N. Rao, Microwave sintering of doped nanocrystalline ZnO and characterization for varistor applications. Mater. Chem. Phys. **115**, 677–684 (2009)
4. S.H. Ko, D. Lee, H.W. Kang, K.H. Nam, J.Y. Yeo, S.J. Hong, C.P. Grigoropoulos, H.J. Sung, Nanoforest of hydrothermally grown hierarchical ZnO nanowires for a high efficiency dye-sensitized solar cell. Nano Lett. **11**, 666–671 (2011)
5. Q. Zhao, T. Xie, L. Peng, Y. Lin, P. Wang, L. Peng, D. Wang, Size-and orientation-dependent photovoltaic properties of ZnO nanorods. J. Phys. Chem. C **111**, 17136–17145 (2007)
6. R. Brayner, R. Ferrari-Iliou, N. Brivois, S. Djediat, M.F. Benedetti, F. Fiévet, Toxicological impact studies based on Escherichia coli bacteria in ultrafine ZnO nanoparticles colloidal medium. Nano Lett. **6**, 866–870 (2006)
7. D. Zhou, A.A. Keller, Role of morphology in the aggregation kinetics of ZnO nanoparticles. Water Res. **44**, 2948–2956 (2010)
8. P. Yang, H. Yan, S. Mao, R. Russo, J. Johnson, R. Saykally, N. Morris, J. Pham, R. He, H.J. Choi, Controlled growth of ZnO nanowires and their optical properties. Adv. Funct. Mater. **12**, 323–331 (2002)
9. S.S. Manoharan, M.L. Rao, Sonochemical synthesis of nanomaterials. ChemInform **35**, 67–82 (2004)
10. P. Banerjee, S. Chakrabarti, S. Maitra, B.K. Dutta, Zinc oxide nano-particles-sonochemical synthesis, characterization and application for photo-remediation of heavy metal. Ultrason. Sonochem. **19**, 85–93 (2012)
11. Y. Chen, Z.G. Chen, X.Z. Li, A.L. Chen, Effect of ultrasonic radiation on preparation of nano-sized CeO_2 powder in alcohol/water reaction system. Chem. Eng. China **35**, 57–60 (2007)
12. Y.L. Wei, P.C. Chang, Characteristics of nano zinc oxide synthesized under ultrasonic condition. J. Phys. Chem. Solids **69**, 688–692 (2008)
13. D.T.N. Anh, H.T.L. Phuong, H.T.H. Thao, N.T.C. Ha, N.X. Hoan, Crystal structures and properties of ZnO nanopowders prepared by ultrasonic method. E-J. Surf. Sci. Nanotechnol. **9**, 482–485 (2011)
14. K.S. Suslick, Sonochemistry. Science **247**, 1439–1445 (1990)
15. X.L. Hu, Y.J. Zhu, S.W. Wang, Sonochemical and microwave-assisted synthesis of linked single-crystalline ZnO rods. Mater. Chem. Phys. **88**, 421–426 (2004)
16. K.S. Suslick, Y. Didenko, M.M. Fang, T. Hyeon, K.J. Kolbeck, W.B. McNamara III, M.M. Mdleleni, M. Wong, Acoustic cavitation and its chemical consequences. Philos. Trans. R. Soc., Math. Phys. Eng. Sci. **357**, 335–353 (1999)
17. I.A. Siddiquey, T. Furusawa, M. Sato, N.M. Bahadur, M. Mahbubul Alam, N. Suzuki, Sonochemical synthesis, photocatalytic activity and optical properties of silica coated ZnO nanoparticles. Ultrason. Sonochem. **19**, 750–755 (2012)
18. R.S. Yadav, P. Mishra, A.C. Pandey, Growth mechanism and optical property of ZnO nanoparticles synthesized by sonochemical method. Ultrason. Sonochem. **15**, 863–868 (2008)
19. S. Zhou, R. Yuan, S. Lou, Y. Wang, H. Yuan, G. Zhu, L. Liu, Y. Hao, N. Li, Sonochemical synthesis and optical properties of amorphous ZnO nanowires. J. Nanopart. Res. **13**, 4511–4518 (2011)
20. H. Zhang, D. Yang, Y. Ji, X. Ma, J. Xu, D. Que, Low temperature synthesis of flowerlike ZnO nanostructures by cetyltrimethylammonium bromide-assisted hydrothermal process. J. Phys. Chem. B **108**, 3955–3958 (2004)
21. R. Hiller, S.J. Putterman, B.P. Barber, Spectrum of synchronous picosecond sonoluminescence. Phys. Rev. Lett. **69**, 1182–1184 (1992)
22. B.P. Barber, S.J. Putterman, Observation of synchronous picosecond sonoluminescence. Nature **352**, 318–320 (1991)
23. Y. Shen, T. Yamazaki, Z. Liu, D. Meng, T. Kikuta, N. Nakatani, Influence of effective surface area on gas sensing properties of WO_3 sputtered thin films. Thin Solid Films **517**, 2069 (2009)
24. X.M. Sun, X. Chen, Z.X. Deng, Y.D. Li, A CTAB-assisted hydrothermal orientation growth of ZnO nanorods. Mater. Chem. Phys. **78**, 99–104 (2003)
25. J.Q. Xu, Y.P. Chen, D.Y. Chen, J.N. Shen, Hydrothermal synthesis and gas sensing characters of ZnO nanorods. Sens. Actuators B **113**, 526–531 (2006)